Available online at www.sciencedirect.com
SCIENCE DIRECT®
Journal of Solid State Chemistry 178 (2005) 3293–3302
JOURNAL OF SOLID STATE CHEMISTRY
www.elsevier.com/locate/jssc

Origin of visible-light-driven photocatalysis: A comparative study on N/F-doped and N–F-codoped TiO_2 powders by means of experimental characterizations and theoretical calculations

Di Li*, Naoki Ohashi, Shunichi Hishita, Taras Kolodiazhnyi, Hajime Haneda

Advanced Materials Laboratory, National Institute for Materials Science (NIMS), 1-1 Namiki, Tsukuba, Ibaraki 305-0044, Japan

Received 20 January 2005; received in revised form 22 June 2005; accepted 14 August 2005
Available online 15 September 2005

Abstract

An overall comparative study was carried out on N-doped, F-doped, and N–F-codoped TiO_2 powders (NTO, FTO, NFTO) synthesized by spray pyrolysis in order to elucidate the origin of their visible-light-driven photocatalysis. The comparisons in their experimentally obtained characteristics were based on the analysis of XPS, UV–Vis, PL, NH_3-TPD and ESR spectra. The comparisons in their theoretically predicted properties were based on the analysis of the calculated electronic structures. As the results, N-doping into TiO_2 resulted in not only the improvement in visible-light absorption but also the creation of surface oxygen vacancies. F-doping produced several beneficial effects including the creation of surface oxygen vacancies, the enhancement of surface acidity and the increase of Ti^{3+} ions. Doped N atoms formed a localized energy state above the valence band of TiO_2, whereas doped F atoms themselves had no influence on the band structure. The photocatalytic tests indicated that the NFTO demonstrated the highest visible-light activity for decompositions of both acetaldehyde and trichloroethylene. This high activity was ascribed to a synergetic consequence of several beneficial effects induced by the N–F-codoping.

Keywords: Anion doping; Titanium dioxide; Photocatalysis; Band structural calculation

1. Introduction

Recently, many attempts have been made in the direction of N, C or S anion-doped TiO_2 photocatalysis because it has good potential for the utilization of the solar energy to eliminate environmental pollutants in air or water [1–3]. However, the most feasible and successful approach among these anions seems to be N-doping, i.e., doping N atoms into the oxygen sites of TiO_2 by calcination in N_2 or NH_3 atmosphere [1,4], wet chemical processes [5,6], spray pyrolysis [7] or other methods [8,9].

The visible-light (Vis)-driven photocatalysis of N-doped TiO_2 powders has been confirmed by many studies. However, two vital problems are still not resolved. One is that the mechanism for exhibiting Vis activity in this system is still controversial. Asahi et al. [1] claimed that the doped N atoms narrow the band-gap of TiO_2 and thus makes it capable of absorbing visible light and demonstrating Vis activity. Irie et al. [4] argued that the isolated narrow band located above the valence band is responsible for the Vis response. In addition, Ihara et al. [5] insisted that it is the oxygen vacancies caused by N-doping that contributed to the Vis activity, and the N dopant only enhances the stabilization of these oxygen vacancies. Another problem is that a significant improvement in the Vis activity of N-doped TiO_2 is needed in order to meet the requirements of practical application because this Vis activity was still in a lower level compared with UV case [1].

F-doping into TiO_2 is also effective for enhancing the photocatalytic activity [10–12]. Yu et al. [10] proposed that the doped F atoms convert Ti^{4+} to Ti^{3+} by charge compensation and that the presence of a certain amount of Ti^{3+} reduces the electron–hole recombination rate and thus enhances the photocatalytic activity. However, they

*Corresponding author. Fax: +81 29 855 1196.
E-mail address: li.di@nims.go.jp (D. Li).

0022-4596/$ - see front matter © 2005 Elsevier Inc. All rights reserved.
doi:10.1016/j.jssc.2005.08.008

did not provide the evidence of Ti^{3+} presence. Hattori et al. [11] interpreted that the enhancement of photocatalytic activity was mainly ascribable to the improvement of TiO_2 crystallinity caused by F-doping. Here, it should be noted that these conclusions were drawn by the study of the photocatalytic reactions under UV irradiation. Recent study confirms that F-doping in TiO_2 can also induce a Vis photocatalytic activity by the creation of oxygen vacancies [12].

Consequently, there is no doubt that N-doping into TiO_2 induces Vis photocatalysis and F-doping enhances the photocatalytic activity for both UV and Vis cases; however, their mechanisms are quite debatable. In our previous study, N-doped, F-doped and N–F-codoped TiO_2 powders were successfully prepared by spray pyrolysis technique [7,12–14]. The most interesting result was that the N–F-codoped TiO_2 powders demonstrated a very excellent photocatalytic activity no matter what kind of light sources (UV or Vis) was used. This seems to be a consequence of the perfect combination of some beneficial effects induced by both N and F dopants. So far, less reports was found for the simultaneous doping of two kinds of anions into TiO_2.

In the present study, an accurately comparative study was carried out on the N-doped, F-doped and N–F-codoped TiO_2 photocatalysts in order to clarify the roles N/F atoms played in the Vis-driven photocatalysis of TiO_2. Attentions were focused not only on their experimentally obtained characteristics but also on their theoretically predicted properties. A computation of the electronic structures was performed for N- and F-doped TiO_2 systems. These findings gained in this study are also helpful for the tailoring of a novel Vis photocatalysts with high performances.

2. Experimental

2.1. Synthesis

N-doped, F-doped, and F–N-codoped TiO_2 powders (NTO, FTO, NFTO) were synthesized by spray pyrolysis (SP) from a mixed aqueous solution of $TiCl_4$ and N-precursor (H_2NCONH_2), F-precursor (HF), or N–F-co-precursor (NH_4F). The mixed solution was first atomized by a nebulizer; then the formed droplets passed through a high-temperature tube under the suction of an aspirator. The pyrolysis proceeded quickly as droplets passed through the high-temperature tube. The produced powder was collected with a ceramic filter at the end of the tube. The temperature of the tube was maintained at 1173 K because the maximum photocatalytic activity was achieved for samples prepared at this temperature [7,12,14]. For comparison, sprayed undoped TiO_2 (TO) powder from a $TiCl_4$ aqueous solution and commercial TiO_2 (Degussa P 25, 50.2 m^2/g, 75% rutile and 25% anatase) were selected as reference samples. The phase composition and surface area of each anion-doped TiO_2 were summarized in Table 1.

2.2. Characterization

The X-ray photoelectron spectra (XPS) measurements were carried out using an ESCALAB 200-X system (VG Scientific) with monochromatic Mg$K\alpha$ excitation and a charge neutralizer, and all the bonding energies were calibrated with the C_{1s} peak at 284.8 eV of the surface adventitious carbon. For XPS measurement, all as-sprayed powders (0.30 g) were pretreated under O_2 flow at 673 K for 2 h in order to completely decompose and remove any possible precursor residues and organic contaminants. The calcined powder was pressed into a disc of 7 mm diameter under a pressure of 100 kg/cm^2. Prior to the XPS measurement, the sample was cleaned by Ar^+ gun. The ion gun settings were: 4 kV, 0.5 μA/cm^2, incident angle of 60°, chamber pressure of 9×10^{-5} Pa (Ar), and sputtering time was 60 min.

The electron spin resonance (ESR) spectra were measured using an ESP-300 spectrometer (Bruker Japan Co., Ltd., Japan) in air at room temperature under Vis ($\lambda > 420$ nm) irradiation. A 150-W Xe lamp (LA-254Xe, $\lambda_{max} = 470$ nm, Hayashi Watch-Works. Co., Ltd, Japan) with a 420-nm cut filter (L42, Kenko, Japan) was used as the Vis sources. Peak positions were corrected using a g-value of 2.0037 for 1,1'-diphenyl-2-picrylhydrazyl (DPPH).

The ultraviolet–visible absorption (UV–Vis) spectra (vs $BaSO_4$) were recorded on a V-550 spectrophotometer (JASCO Co., Japan) with an integrating sphere. The photoluminescence (PL) spectra were measured at room

Table 1
Physical parameters and photocatalytic activities of the anion-doped TiO_2 powders

Sample	Phases	Surface area[a] (M^2/g)	Total-N (at%)	Site-N (at%)	Total-F (at%)	Site-F (at%)	Acid sites (μmol/m^2)	AAH adsorbed (μmol/m^2)	R_0, AAH (TCE) (10^{-7} mol/min)
FTO	A	19.8			1.08	0.29	1.20	1.9	1.02 (—)
NTO	A	23.1	0.81	0.22			0.20	0.26	0.45 (0.34)
NFTO	A	102	0.61	0.18	1.35	0.40	0.88	1.5	1.67 (1.25)
TO	A + R	5.0					0.31	0.35	0.049 (0.033)
P 25	A + R	50.2					0.68	0.86	0.28 (0.069)

A and R denote anatase and rutile, respectively.
[a]Calculated from N_2 adsorption isotherms at 77 K.

temperature using an RPM2000 spectrophotometer (ACCENT Semiconductor Technologies Ltd., UK) with a He–Cd laser ($\lambda = 325$ nm) as the light source. The NH_3 temperature-programmed desorption (NH_3-TPD) profile was obtained using a TPD-1-TA instrument (BEL Japan, Inc.). The sample of 0.100 g was evacuated at 673 K for 1 h, and then the bed temperature was cooled down to 373 K. After that, NH_3 (6.4×10^{-4} mol) was introduced and kept the sample for NH_3 adsorption at 373 K for 0.5 h, and the gaseous NH_3 was then evacuated. The bed temperature was elevated to 1173 K at a rate of 10 K min^{-1}. The desorbed NH_3 was detected by a quadruple mass analyzer.

2.3. Computational methods

The first-principle calculations were based on the plane-wave pseudo-potential method [15] within the generalized gradient approximation [16]. The self-consistent total energy in the ground state was effectively obtained by the density-mixing scheme [17]. Atomic positions were optimized to minimize the total energy using the quasi-Newton method with the Broyden–Fletcher–Goldfard–Shanno Hessian update scheme [18]. The ultrasoft pseudo-potentials [19] were applied for efficient computation, and the kinetic-energy cutoff was set to 380 eV. A $2 \times 2 \times 2$ supercell, including 16 atoms of Ti-sites and 32 atoms of O-sites, was considered to model for anatase. Firstly, lattice parameters and fractional atomic coordinates for perfect anatase lattice were evaluated, and the lattice parameters of the super-cell including impurity was fixed at same values corresponding to the perfect cell. For calculation of super-cell, a $3 \times 3 \times 2$ mesh of k points was used to sample the Brillouim zone and $50 \times 50 \times 64$ mesh was used for fast Fourier transformation. The convergences were set to less than 2×10^{-4} nm for displacement and 2×10^{-6} eV/atom for total energy difference. All calculations were performed by the software CASTEP (Accelrys Software Inc., San Diego, USA). For modeling of the F/N-doped anatase, an F/N atom was substituted for one of 32 O atoms. During structural optimization, any constraints were assumed: namely, all the atoms were relaxed. In the present study, both N and F were assumed to be a cause of neutral donor in anatase. It should be also noted that electron spin polarization was not considered in the present calculations because of limitation of calculation resources.

2.4. Photocatalytic activity measurements

Decompositions of the acetaldehyde and trichloroethylene were used as probe reactions to evaluate the photocatalytic activities of the anion-doped TiO_2 powders. Photocatalytic reaction was carried out in a closed circulation system (CCS) interfaced to a gas chromatograph for analysis of the gas composition. Prior to the photocatalytic test, the photocatalyst (0.600 g) was treated at 673 K for 2 h in air to remove any adventitious organic impurities. Then, the accurately weighted photocatalyst (0.500 g) was rapidly placed into a home-made reactor cell connected with the CCS. The sample was evacuated under a pressure of 10^{-5} Pa at room temperature for 1.0 h. A gas mixture of 101.3 kPa O_2/N_2 (v/v = 21/79) containing 930 ppm CH_3CHO or 943 ppm $CHCl{=}CCl_2$ was introduced into the CCS. The samples were irradiated from inside of the reactor, which was described elsewhere [14]. A group of blue light-emitting diode (LED) lights embedded into a panel (DC 12 V × 0.4 A, $\lambda_{max} = 470$ nm, Koha Co., Ltd, Japan) was used as a Vis source. The incident intensity of the light to the sample surface was about 4 mW cm^{-2}. Here, it should be noted that the pretreatment of the photocatalyst is indispensable for the correct evaluation of activity, because the photocatalyst can adsorb the organic substances in air during its storage even if it was prepared at high temperature. In this study, we found that the amount of CO_2 formation was always much higher than the double amount of the introduced acetaldehyde for an as-prepared sample, sometimes, the CO_2 yield was up to 180%.

3. Results and discussion

3.1. Vis-driven photocatalytic activity

3.1.1. Photocatalytic decomposition of acetaldehyde (AAH)

The CO_2 evolution from AAH decomposition over the anion-doped TiO_2 powders with blue LED irradiation is given in Fig. 1. The following conclusions can be drawn. (1) The anion-doped TiO_2 powders demonstrated high photocatalytic activities. They were much higher than the

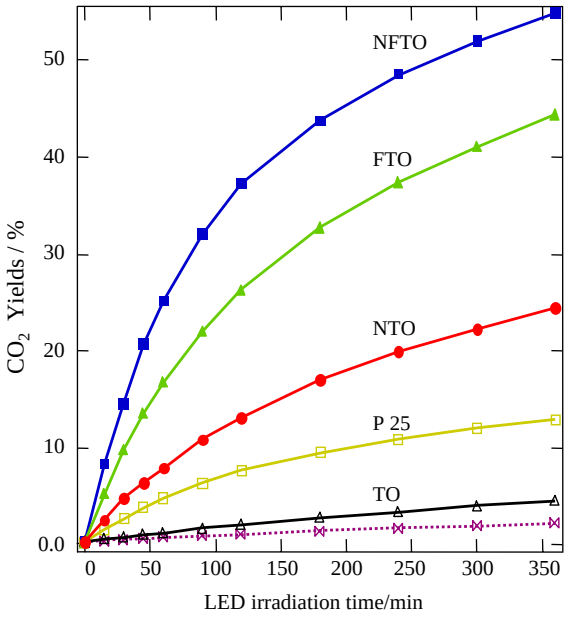

Fig. 1. CO_2 evolution during the AAH decomposition on the anion-doped TiO_2 powders. The dotted line represents the blank test without photocatalyst.

activities of the reference samples, such as P 25 or TO. (2) The photocatalytic activity of the anion-doped TiO_2 powders greatly depended on dopant component; the maximum photocatalytic activity was observed for NFTO with N–F-codoping. (3) N-doping alone could not significantly improve the Vis photocatalysis of TiO_2, which was inferred by comparing the photocatalytic activity of NTO with TO. However, F-doping alone gave a significant enhancement in photocatalytic activity, which was deduced by comparing the photocatalytic activity of FTO with TO. As a result, N–F-codoping is the most effective approach for achieving a Vis-driven photocatalysis. In this study, the initial rate (R_0, mol/min) of CO_2 formation, 3.0 h after the reaction began, were calculated to represent the photocatalytic activity in order to make a quantitative comparison. The results are listed in Table 1. The R_0 value of NFTO was much higher than that of TO by 34 times, and of P 25 by six times. The Vis-driven photocatalysis induced by the N–F-codoping was outstanding.

3.1.2. *Photocatalytic decomposition of trichloroethylene (TCE)*

In order to further verify the reliability of the Vis photocatalytic activity of the anion-doped TiO_2 powders, the photocatalytic decomposition of TCE was also investigated. The results are given in Fig. 2; their R_0's of CO_2 formation are given in Table 1. These results are similar to those of the AAH case, NFTO powder demonstrated the highest photocatalytic activity among the tested samples. Here, it should be pointed out that TCE generally cannot be degraded into CO_2 under only Vis irradiation; however, it was effectively degraded over the FTO and NFTO. This further confirmed the unique photocatalytic property of our anion-doped TiO_2 samples for the mineralization of organic pollutants.

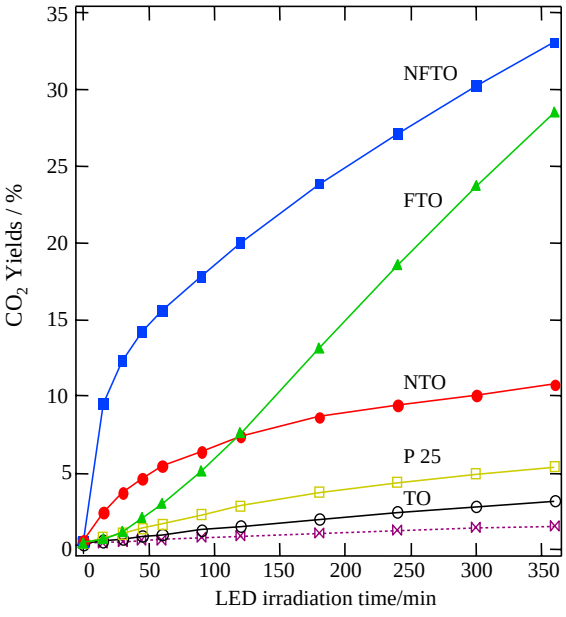

Fig. 2. CO_2 evolution during the TCE decomposition on the anion-doped TiO_2 powders. The dotted line represents the blank test without photocatalyst.

Furthermore, a big difference in the shapes of the CO_2 evolution curves was observed. An obvious "promoted period" for CO_2 formation was observed for NFTO at the beginning of the reaction; contrarily, an obvious "induced period" was observed for FTO. However, these phenomena did not appear in the AAH case, indicating that the photocatalytic decomposition of TCE seemed to be a structure sensitive reaction [20]. It is well known that hydroxyl ($OH^\bullet$) radicals, generated via hole capture by surface hydroxyl or water molecules, and superoxide ($O_2^{\bullet -}$) radicals, generated via electron capture by adsorbed oxygen, are responsible for the photocatalytic decomposition of organic pollutants [21,22]. The AAH decomposition on TiO_2 is mediated by both $OH^\bullet$ and $O_2^{\bullet -}$ radicals [23]. However, it seems to be extremely complex for the TCE decomposition. $OH^\bullet$ radicals might play an important role for the TCE decomposition on the FTO powder because the presence of the "induced period" implies that the water molecules formed during the reaction initiation was important for initiating TCE decomposition, especially when TCE decomposition was carried out in water-free air atmosphere like in our case. On the other hand, $O_2^{\bullet -}$ radicals might be mainly responsible for the TCE decomposition on the NTO or NFTO because of the presence of the "promoted period". The reasons invoked in this difference are our further interest.

Finally, it should be noted here that the reactor cell used in this study was specially designed by simulating a commercial LED air cleaner used in cars [14]. It cannot only be used to evaluate the performances of a photocatalyst but also provide the information on its potentials for application to air purification. Therefore, the NFTO photocatalyst has good potential for implementation.

3.2. *Origin of the Vis activity of the anion-doped TiO_2 powders*

3.2.1. *Chemical states of N and F atoms*

The chemical forms and concentrations of the N and F atoms in their corresponding samples were investigated through the analysis of XPS spectra. Fig. 3a shows the N_{1s} XPS spectra of the anion-doped TiO_2 powders after 60 min Ar^+ sputtering. The reason for the selection of 60 min sputtering was described elsewhere [13]. Two peaks, peak 1 at 400 eV and peak 2 at 396.5 eV, were observed for NTO and NFTO. Relatively, only one broad peak centered at 400 eV was found for FTO. This indicates that appearances of peaks on the NTO and NFTO mainly originated from the intentionally added N-precursors. The very weak trace of the peak in the spectrum of FTO should originate from N_2 in air since no N-source was used during the FTO preparation. The peak 1 was assignable to the N atoms from molecularly adsorbed N-containing compounds (e.g., NH_3 and NO_x) [24,25], which formed during the decomposition and oxidation of the N-precursors. Peak 2 is

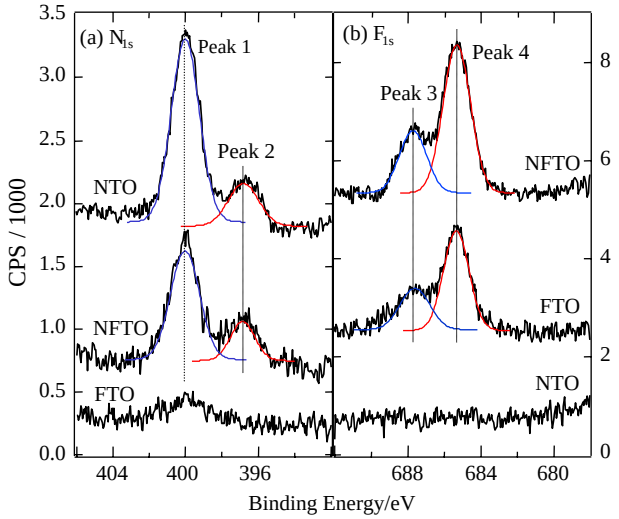

Fig. 3. XPS spectra of N_{1s} (a) and F_{1s} (b) for the anion-doped TiO_2 powders after 60 min Ar^+ sputtering.

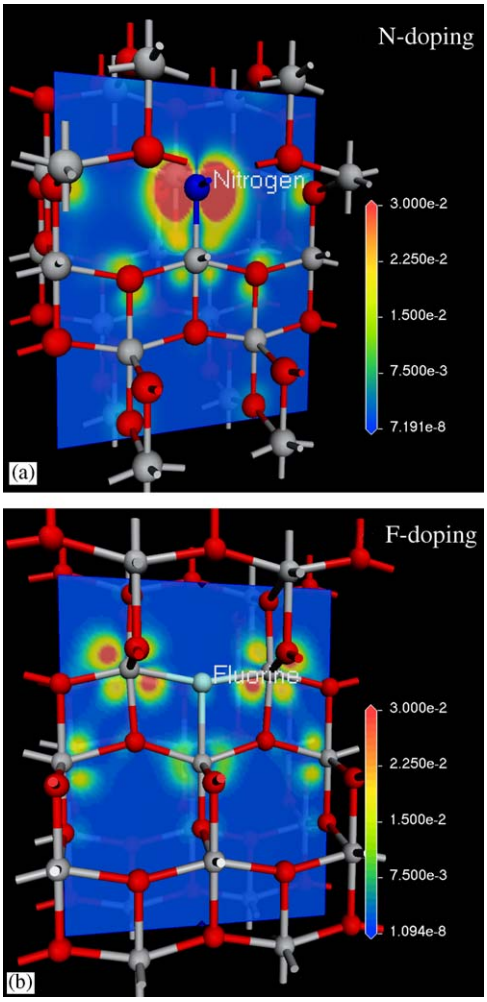

Fig. 4. Electron density maps of the N-doped (a) and F-doped TiO_2 (b).

generally considered as the evidence for the presence of Ti–N bonds formed when N atoms replace the oxygen in TiO_2 crystal lattice [1,4,6,24]. Here, these N atoms are called site-N.

Fig. 3b shows the F_{1s} XPS spectra of the anion-doped TiO_2 powders after 60 min Ar^+ sputtering. Peak 3 located at 687.8 eV was attributed to the substitutional F atoms in TiO_2 crystal lattice [10,12]. Here, these F atoms are called site-F. Peak 4 located at 685.3 eV was attributed to the F atoms of the $TiOF_2$ [12,13]. Moreover, no F trace was found in the XPS spectra of NTO and TO, indicating that the F atoms in the FTO and NFTO powders originated from their corresponding F-precursors and not from contaminants.

Based on these XPS results, the concentrations of the total-N/F and site-N/F atoms in the anion-doped TiO_2 powders were calculated. The results are listed in Table 1. The site-N concentrations were 0.22 at% for NTO and 0.18 at% for NFTO; the site-F concentrations were 0.29 at% for FTO and 0.40 at% for NFTO. Additionally, it is worth to note that most of the F atoms in the FTO and NFTO powders were present mainly in the form of $TiOF_2$. The contents of $TiOF_2$ calculated from the difference between total-F and site-F concentrations were 1.54 weight% (wt%) for FTO and 1.85 wt% for NFTO.

3.2.2. *Calculation of the electronic structures for N/F-doped TiO_2*

The lattice parameters of undoped anatase were predicted to be $a = 3.786$ and $c = 9.722$ Å with the structural relaxation to minimize the inter-atomic force and total energy. The c-parameter was about 2% larger than the experimentally obtained lattice parameters of anatase ($a = 3.785$ and $c = 9.514$ Å, JCPDS-ICDD No 21-1272), we can say that the predicted crystal structure of anatase is in good agreement with the experimental one. Fig. 4 illustrates the results of structural optimization for N-doped and F-doped super-lattices as well as the electron density maps (EDM) corresponding to the highest occupied states. Firstly, the N/F incorporation into anatase did not result in a significant change in the structure because an obvious reconstruction was not found in these figures. The Ti–N bond length (1.940 and 2.042 Å) and the Ti–F bond length (2.022 and 2.253 Å) are only slightly longer than the Ti–O ones (1.940 and 2.000 Å). Therefore, the electronic structural changes due to the geometric modifications are minor. Secondly, the inclusion of an N atom in the lattice resulted in a paramagnetic impurity (Fig. 4a). The unpaired electron has a strong N_{2p} character, and is largely localized at N site, with small tails extending on the neighbor O atoms. This is a conclusive evidence for the localized nature of electron state formed by N impurity. On the other hand, the inclusion of an F atom in the lattice resulted in a high delocalization of the electron density at F site; instead, the electron density of the neighbor Ti atom was enhanced.

The partial densities of state (DOS) of pure, N-doped and F-doped anatase are plotted in Fig. 5. The calculated energy band-gap of pure anatase was less than the

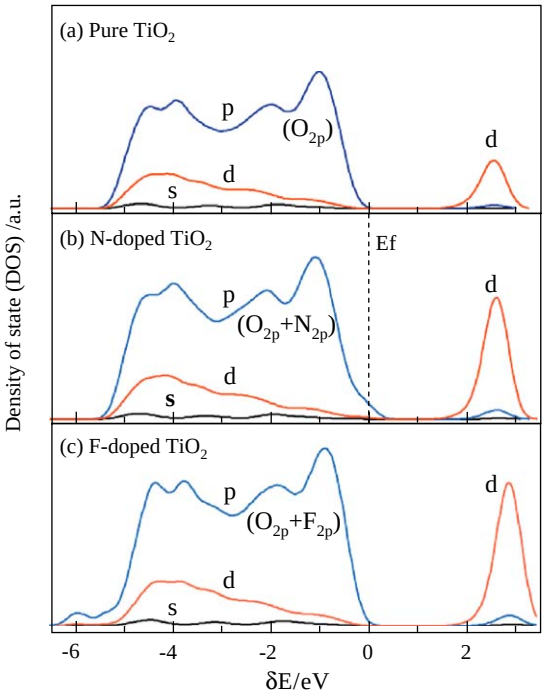

Fig. 5. Partial DOS's of the pure (a), N-doped (b) and F-doped TiO_2 (c).

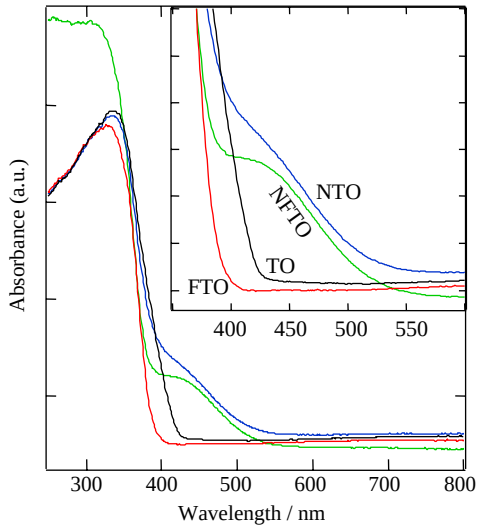

Fig. 6. UV–Vis adsorption spectra of the anion-doped TiO_2 powders. The inset shows the enlargement of a part of the adsorption spectra ranging from 350 to 600 nm.

experimentally observed value due to density functional approximation. The valence band (VB) is dominated by O_{2p} and the conduction band (CB) Ti_{3d}. N_{2p} DOS appeared on the top of the VB (Fig. 5b) with a mixing with that of O_{2p}, which was drawn from the comparison of total DOS of O_{2p} and N_{2p} with the O_{2p} DOS of pure anatase (Fig. 5a). This result seems to conclude that N-doping narrowed the band-gap of TiO_2, as claimed by Asahi et al. [1]. However, it should be emphasized that this narrow band-gap only corresponds to a substance, $Ti_{16}O_{31}N$, in which the N concentration is up to 2.08 at%. It was much higher than that in our experimental samples (NTO and NFTO) by 10 times. Therefore, it is reasonable to consider that N-doping induced a localized energy state above the VB (as indicated in Fig. 4a) rather than the narrowing of the band-gap of TiO_2. F_{2p} DOS appeared on the bottom of the VB (Fig. 5c) with less mixing with that of O_{2p}. Consequently, it cannot be expected to influence the optical absorption property of TiO_2.

3.2.3. N and F roles

N-doping improves the Vis absorption of TiO_2. The UV–Vis absorption spectra of the anion-doped TiO_2 powders are shown in Fig. 6. Compared with the optical adsorption of anatase TiO_2 (3.20 eV), TO (3.0 eV) showed a slight red-shift because it contained rutile phase in addition to anatase (Table 1). For the case of FTO (3.19 eV), the optical absorption appeared to be not affected by the F-doping. This conclusion is completely consistent with the results of the above-mentioned as well as reported calculations for F-doped TiO_2 system [1,26,27]. However, for NTO and NFTO, a new absorption band was observed in the visible range of 400–550 nm in addition to the fundamental absorption edge of TiO_2. This new absorption band was attributed to the doped N atoms [1,4–9,14]. Additionally, the Vis absorption intensity was in a direct proportion with their site-N levels, a stronger Vis absorption was observed for the NTO with the higher site-N concentration.

N/F-doping contributes the creation of oxygen vacancies. Fig. 7a shows the PL spectra of the anion-doped TiO_2 powders. A broad band was observed for each tested sample. However, according to the characteristics of the PL spectra of NFTO and FTO in curve shape, the PL spectrum of NFTO or NTO was deconvoluted into five peaks (Fig. 7b); the PL spectrum of FTO was deconvoluted into three peaks, and the latter three peaks were among the former five peaks in position. Peak 1 at 465 nm was attributed to the oxygen vacancy (OV) with two trapped electrons, i.e., F center, and peak 2 at 525 nm was assigned to the OV with one trapped electron, i.e., F^+ center [28,29]. Peak 3 at 627 nm might be a consequence of the Franck–Condon principle and the polarizability of the lattice ions surrounding the vacancy, the emitting center was identified as Ti^{3+} ions [29]. However, the energy state induced by Ti^{3+} ions seems to locate just below the CB of TiO_2 [10]. Therefore, in this study, peak 3 is considered as an origin-unidentified peak. Peak 4 at 700 nm was originated from doped N atoms because such a peak was only observed for N-doped NTO and NFTO; thus it should be closely related to impurity energy state (IES) caused by N-doping. This conclusion was also supported by our calculated results (Fig. 4a)

Based on the analysis of these PL results, we propose a structural model in Fig. 8 for the energy states existing between the VB and CB of the TiO_2 with N–F-codoping.

The excited electron transition pathways corresponding to each peak is also illustrated there. Shallow traps at 0.53 eV for F center and 0.84 eV for F^+ center below the CB correspond to peak 1 and peak 2, respectively. These values agree well with the reported F and F^+ center levels in TiO_2 [28–30]. Deep traps at 2.0 eV for an origin-unidentified energy state (OUES) and 2.6 eV for IES below the CB correspond to peak 3 and the absorption edge (475 nm) in visible region for NFTO, respectively. This IES level was also confirmed from the results on the electronic structural calculation. In addition, PL spectra also directly reveal the processes of the radiative recombination of charge carriers between two different energy states [29]. Therefore, the peak 4 was assigned to the transfer of excited electrons between F^+ center and IES. Peak 5 at 905 nm was assigned to the transfer of excited electrons between F center and OUES. The PL intensity of NTO was higher than that of TO or P 25, indicating that N-doping resulted in the creation of OVs. However, F-doping led to a more pronounced enhancement of OVs by the comparison of FTO and TO, or NFTO and NTO.

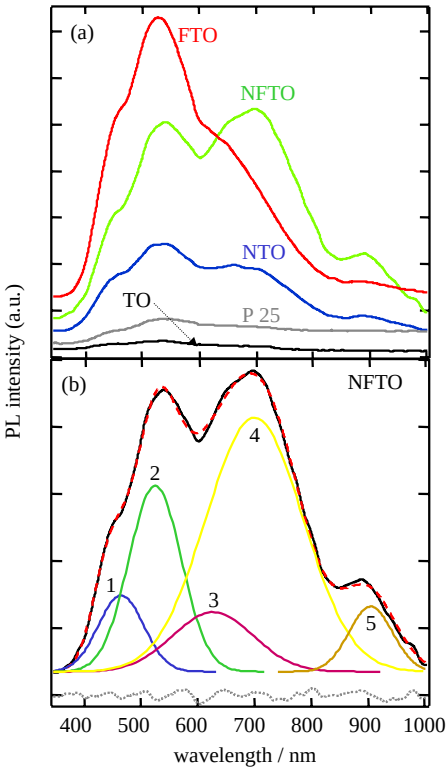

Fig. 7. (a) PL spectra of the anion-doped TiO_2 powders. (b) The deconvolution of the broad peak for NFTO. The solid line represents the original TPD profile and deconvoluted peaks, the broken line is fitting curve, and the dotted line is the error of the fitting.

F-doping promotes the formation of surface acid sites. The surface acidities of the anion-doped TiO_2 powders were evaluated by NH_3-TPD measurement. The results are shown in Fig. 9. The NH_3 desorption profiles depended significantly on the dopants. Less ammonia desorption was observed for TO and NTO; while a broad desorption peaks were found for FTO and NFTO. These indicate that only N-doping cannot lead to the formation of surface acid sites. The F-doping is responsible for the surface strong acidity of FTO and NFTO. The TPD profiles with a broad peak were deconvoluted into two peaks with Gaussian distributions. The first peak was attributed to the weak NH_3 adsorption; the second peak was attributed to NH_3 adsorption on the acid sites. Accordingly, the second peak

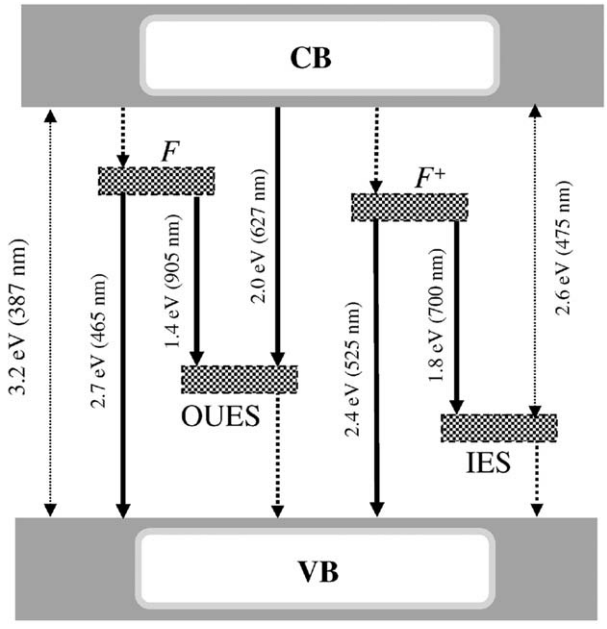

Fig. 8. Proposed structural model of energy states that exist between the VB and CB of the TiO_2 with N–F-codoping. The dotted arrows represent the possible existing PL emissions beyond 1000 nm.

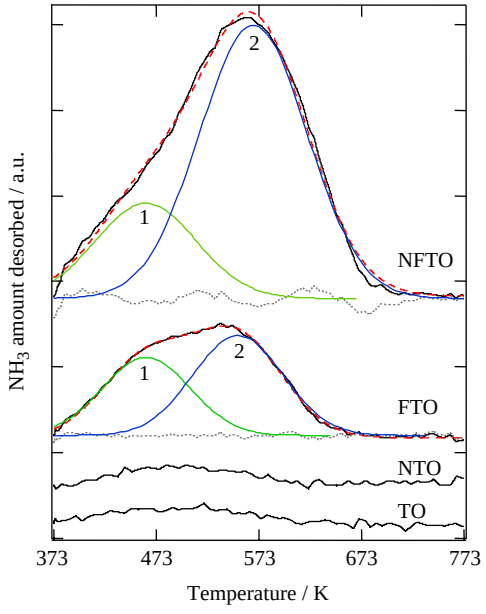

Fig. 9. NH_3-TPD profiles for the anion-doped TiO_2 powders. The solid line represents the original TPD profile and deconvoluted peaks, the broken-dotted line is fitting curve, and the dotted line is the error of the fitting.

was used to represent the surface acidities of the tested samples, which are given in Table 1. The FTO and FNTO with F-doping demonstrated the very strong surface acidities compared with that of TO. It is reported that acidic surface could enhance the adsorptivity of a photocatalyst for a reactant [31]. Therefore, AAH amounts adsorbed on these anion-doped TiO_2 powders were measured using a previously described method [14]. The results are shown in Table 1. Undoubtedly, the FTO or NFTO with a strongly acidic surface adsorbed more AAH molecules.

F-doping induces the formation of Ti^{3+} ions. The ESR spectra of the anion-doped TiO_2 powders are shown in Fig. 10. The measurements were carried out in air at room temperature under the Vis irradiation in order to maintain the consistent conditions with the photocatalytic reactions. A weak and symmetric signal was observed for TO, whereas some strong signals were found for the anion-doped TiO_2. The signals were not ascribed completely; however, the signals with *g*-factors of 2.003 and 2.016 were unambiguously assigned to the $O_2^{\bullet -}$ adsorbed on the surface of anatase TiO_2 because it was regarded as the only radical stable at room temperature [32,33]. Anion-doping, especially F-doping, significantly enhanced the formation of the $O_2^{\bullet -}$. The amount of the $O_2^{\bullet -}$ for each tested sample appeared to be proportional with that of its OVs on an assumption that strong PL intensity means more OVs. The signals with *g*-factors of 1.963 and 1.991 were assigned to the Ti^{3+} ions [34]. From the comparison of FTO and TO or NFTO and NTO, it can be understood that the F-doping promoted significantly the formation of Ti^{3+} ions.

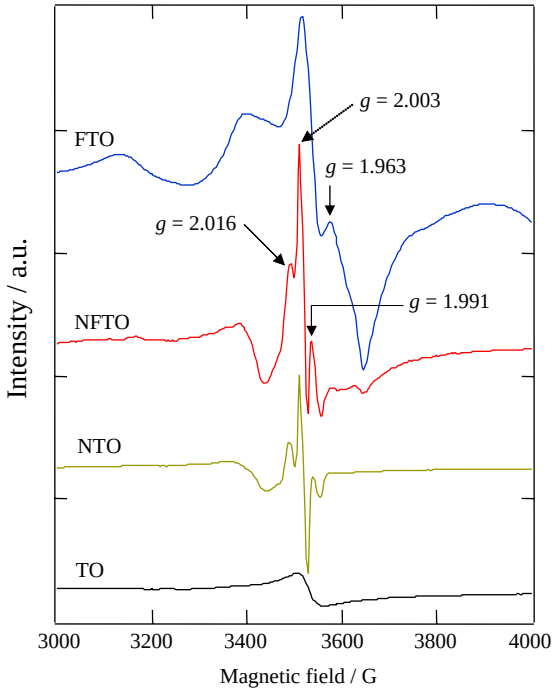

Fig. 10. ESR spectra of the anion-doped TiO_2 powders. The measurements were carried out in air at room temperature under Vis (>420 nm) irradiation.

This conclusion well agrees with the calculated result (Fig. 4b), in which F-doping implied a transformation from antimagnetic Ti^{4+} to paramagnetic Ti^{3+}. Yu et al.[10] also explained the formation of Ti^{3+} ions through the charge compensation between F^- and Ti^{4+} .

3.2.4. Origin of the Vis activity of the anion-doped TiO_2 powders

Overall comparative study on NTO, FTO and NFTO, the effects of N/F-doping on the intrinsic characteristics of TiO_2 are explicit. Therefore it is easy to elucidate the origin of the Vis activity over these anion-doped TiO_2 powders. For the NTO, N-doping resulted in not only the improvement in Vis absorption but also the creation of surface OVs. By comparing the activity of N-alone-doped NTO with undoped TO, N-doping really increased the Vis photocatalysis. The UV–Vis spectra in Fig. 6 unequivocally indicate that the N-doping did not cause the narrowing of the band-gap of TiO_2 because a shift in the fundamental absorption edge of TiO_2 was not observed. This indicates that the intrinsic redox ability of TiO_2, governed by the relative positions of CB and VB [35], was not affected by the N-doping. Instead, an isolated IES (Fig. 8) was formed above the VB. The presence of this IES improved the Vis absorption and thus increased the number of photons taking part in the photocatalytic reaction. Undoubtedly, this could enhance the Vis photocatalysis. However, it should be pointed out that such an IES also has a double-faced behavior. Except for the positive role, the IES can also act as a recombination center of photo-generated charge carriers, and thus deteriorates photocatalysis [14]. The suppression in the UV activity of the N-doped TiO_2 photocatalyst was just an experimental evidence for the negative role [1]. Additionally, even in Vis-driven photocatalysis, an appropriate site-N concentration seems to be dispensable for achieving a higher activity because a high site-N level may produce a diminishing return in activity due to the play of the negative role [4,7,14]. On the other hand, N-doping resulted in the creation of surface OVs. It is well known that OVs in/on a solid will make the spectral limit of a surface photochemical process red-shift to visible region [36–38]. The decomposition of organic pollutants by the VOs-induced Vis photocatalysis were also reported [12,39]. Further, the enhancement in visible-excited photocurrent in the sites of OVs was virtually confirmed by STM studies of the TiO_2 (110) surface [40]. The pathway of the achievement of this Vis photocatalysis is that OVs act as the active sites for the formation of the $O_2^{\bullet -}$ and $OH^{\bullet}$ radicals [41,42]. Consequently, the appearance of the Vis activity of NTO is ascribed to both the improvement of Vis absorption and the creation of surface OVs.

For the FTO, the creation of surface OVs was considered as the origin of the Vis photocatalysis [12]. Fig. 6 indicates that F-doping did not cause a pronounced change in intrinsic optical absorption of TiO_2. However, the PL spectra and their analysis in Figs. 7 and 8 confirmed the enhancement of the OVs by F-doping. Therefore, the

decompositions of AAH and TCE on the FTO under Vis irradiation should be a consequence of the excitation of the absorption bands of these extrinsic OVs rather than the excitation of intrinsic absorption band of bulk TiO_2. Moreover, this OVs-induced Vis activity was further improved by the strongly acidic surface and Ti^{3+} ions. The correlations among the surface acidity, AAH amount adsorbed, and photocatalytic activity were described in detail elsewhere [14]. In addition, the surface acidic sites also act as an electron acceptor [43], which would enhance the separation of photo-generated charge carriers and improve the photocatalytic efficiency. As for the Ti^{3+} ions, Yu et al. [10] claimed that the existence of a certain amount of Ti^{3+} ions in TiO_2 reduced the recombination rate of the photo-generated electrons and holes and thus enhanced the photocatalytic activity. Consequently, several beneficial effects produced by F-doping were ascribed to the higher Vis activity of FTO.

With the accurate elucidation on the origins of the Vis photocatalysis for NTO and FTO, the reasons for exhibiting the excellent Vis activity over the NFTO was clear at a glance. The high activity of NFTO should be a combined consequence of some beneficial effects induced by the N–F-codoping. These effects include the improvement of Vis absorption, the creation of surface OVs, the enhancement of surface acidity, and the increase of Ti^{3+} ions.

4. Conclusions

The roles of N and F atoms were clearly elucidated through an overall comparative study on the N/F-doped and N–F-codoped TiO_2 powders. N-doping resulted in not only the improvement in Vis absorption but also the creation of surface OVs. F-doping produced several beneficial effects: the creation of surface OVs, the enhancement of surface acidity and the increase of Ti^{3+} ions. NFTO demonstrated the highest Vis activity for the decompositions of both AAH and TCE, being much high than that of commercial P 25. This high activity was ascribed to a synergetic consequence of several beneficial effects induced by the N–F-codoping. TiO_2 photocatalysis is governed by many factors; the perfect integration of these factors should be a vital step for the tailoring of a novel Vis-driven photocatalyst.

Acknowledgments

This research is part of the Millennium Project for the "Search and Creation of a Catalyst for Removing Harmful Chemical Substances" sponsored by the Ministry of Education, Culture, Sports, Science and Technology (MEXT), Japan. This study was also partly supported by Industrial Technology Grant Program (ID04A26018) from New Energy and Industrial Technology Development Organization (NEDO), Japan. Here, we are grateful for the financial support.

References

[1] R. Asahi, T. Morikawa, T. Ohwaki, K. Aoki, Y. Taga, Science 293 (2001) 269.
[2] S.U.M. Khan, M. Al-Shahry, W.B. Ingler, Science 297 (2002) 2243.
[3] T. Ohno, M. Akiyoshi, T. Umebayashi, K. Asai, T. Mitsui, M. Matsumura, Appl. Catal. A: Gen. 265 (2004) 115.
[4] H. Irie, Y. Watanaba, K. Hashimoto, J. Phys. Chem. B 107 (2003) 5483.
[5] T. Ihara, M. Miyoshi, Y. Iriyama, O. Matsumoto, S. Sugihara, Appl. Catal. B: Environ. 42 (2003) 403.
[6] J.L. Gole, J.D. Stout, C. Burda, Y. Lou, X. Chen, J. Phys. Chem. B 108 (2004) 1230.
[7] D. Li, H. Haneda, S. Hishita, N. Ohashi, Mater. Sci. Eng. B 117 (2005) 67.
[8] S. Yin, H. Yamaki, M. Komatsu, Q. Zhang, J. Wang, Q. Tang, F. Saito, T. Sato, J. Mater. Chem. 13 (2003) 2996.
[9] T. Sano, N. Negishi, K. Koike, K. Takeuchi, S. Matsuzawa, J. Mater. Chem. 14 (2004) 380.
[10] J.C. Yu, J. Yu, W. Ho, Z. Jiang, L. Zhang, Chem. Mater. 14 (2002) 3808.
[11] A. Hattori, K. Shimota, H. Tada, S. Ito, Langmuir 15 (1999) 5422.
[12] D. Li, H. Haneda, S. Hishita, N. Ohashi, N.K. Labhsetwar, J. Fluorine Chem. 126 (2005) 69.
[13] D. Li, H. Haneda, S. Hishita, N. Ohashi, Chem. Mater. 17 (2005) 2588.
[14] D. Li, H. Haneda, S. Hishita, N. Ohashi, Chem. Mater. 17 (2005) 2596.
[15] V. Milman, B. Winkler, J.A. White, C.J. Pickard, M.C. Payne, E.V. Akhmatskaya, R.H. Nobes, Int. J. Quantum Chem. 77 (2000) 895.
[16] J.P. Perdew, J.A. Chevary, S.H. Vosko, K.A. Jackson, M.R. Pederson, D.J. Singh, C. Fiolhais, Phys. Rev. B 46 (1992) 6671.
[17] G. Kresse, J. Furthmüller, Phys. Rev. B 54 (1996) 169.
[18] W.H. Press, S.A. Teukolsky, W.T. Vetterling, B.P. Flannery, Numerical Recipes, second ed, Cambridge University Press, Cambridge, 1992, p. 418.
[19] K. Laasonen, R. Car, C. Lee, D. Vanderbilt, Phys. Rev. B 43 (1991) 6796.
[20] J.N. Wilson, H. Idriss, J. Am. Chem. Soc. 124 (2002) 11284.
[21] M.R. Hoffmann, S.T. Martin, W. Chio, D.W. Bahnemann, Chem. Rev. 95 (1995) 69.
[22] A. Fujishima, T.N. Rao, D.A. Tryk, J. Photochem. Photobiol. C: Photochem. Rev. 1 (2000) 1.
[23] I. Sopyan, M. Watanabe, S. Murasawa, K. Hashimoto, A. Fujishima, J. Photochem. Photobiol. A: Chem. 98 (1996) 79.
[24] N.C. Saha, H.G. Tompkins, J. Appl. Phys. 72 (1992) 3072.
[25] C.D. Wagner, W.M. Riggs, L.E. Davis, J.F. Moulder, in: G.E. Muilenberg (Ed.), Handbook of X-ray Photoelectron Spectroscopy, Perkin-Elmer Co., Minnesota, 1979.
[26] A. Stashans, S. Lunell, R.W. Grimes, J. Phys. Chem. Solids 57 (1996) 1293.
[27] T. Yamaki, T. Umebayashi, T. Sumita, S. Yamamoto, M. Maekawa, A. Kawasuso, H. Itoh, Nucl. Instrum. Meth. In Phys. Res. B. 306 (2003) 254.
[28] Y. Lei, L.D. Zhang, G.W. Meng, G.H. Li, X.Y. Zhang, C.H. Liang, W. Chen, S.X. Wang, Appl. Phys. Lett. 78 (8) (2001) 1125.
[29] N. Serpone, D. Lawless, R. Khairutdinov, J. Phys. Chem. 99 (1995) 16646.
[30] L.V. Saraf, S.I. Patil, S.B. Ogale, S.R. Sainkar, S.T. Kshirsager, Int. J. Mod. Phys. B 12 (1998) 2635.
[31] V. Keller, P. Bernhardt, F. Garin, J. Catal. 215 (2003) 129.
[32] P. Meriaudeau, J.C. Vedrine, J. Chem. Soc., Faraday Trans. II 72 (1976) 472.
[33] R.F. Howe, M. Grätzel, J. Phys. Chem. 91 (1987) 3906.
[34] R.F. Howe, M. Grätzel, J. Phys. Chem. 89 (1985) 4495.
[35] A.L. Linsebigler, G. Lu, J.T. Yates, Chem. Rev. 95 (1995) 735.

[36] A.V. Emiline, G.V. Kataeva, V.K. Ryabchuk, N. Serpone, J. Phys. Chem. B 103 (1999) 9190.
[37] A.V. Emiline, G.N. Kuzmin, D. Purevdorj, V.K. Ryabchuk, N. Serpone, J. Phys. Chem. B 104 (2000) 2989.
[38] A.M. Volodin, Catal. Today 58 (2000) 103.
[39] I.N. Martyanov, S. Uma, S. Rodrigues, K.J. Klabunde, Chem. Commun. (2004) 2476.
[40] M. Komiyama, Y. Li, Jpn. J. Appl. Phys. 43 (2004) 4584.
[41] M.A. Henderson, W.S. Epling, C.L. Perkins, C.H.F. Peden, J. Phys. Chem. B. 103 (1999) 5328.
[42] R. Schaub, P. Thostrup, N. Lopez, E. Lægsgaard, I. stensgaard, J.K. Nørskov, F. Besenbacher, Phys. Rev. Lett. 87 (2001) 266104.
[43] S.R. Morrison, Surf. Sci. 50 (1975) 329.